Ion Beam Modification of Poly (methyl methacrylate) (PMMA)

Raquel Silva Thomaz and Ricardo Meurer Papaléo

Abstract In this chapter, we review fundamental issues related to the damaging processes of PMMA films induced by high-energy ions with kinetic energies from a few keV to a few GeV, covering the regimes of energy deposition dominated by nuclear collisions and by electronic excitation. Emphasis is given to present an overview of the bond-breaking processes, the changes in the polymer chemical structure, and the corresponding modifications in selected macroscopic physical properties (optical, mechanical, and electrical).

Keywords Ion beam · PMMA · Physicochemical properties · Mechanical properties

1 Introduction

Poly(methyl methacrylate) (PMMA) is one of the most important polymeric materials available commercially. Due to its excellent mechanical properties, chemical resistance, and optical behavior similar to glass, it has been widely utilized across several industries, mainly as shatterproof windows, illuminated signs, and optical parts, but also as a structural material for different electronic, construction, and household goods [1]. The high biological compatibility made PMMA a common material for biomedical applications in ophthalmology, prosthetics, orthopedics, and dentistry, to name a few [2]. Resins based on PMMA have also been widely used in microlithography with UV photons, X-rays, or electron beams [3–6], or in direct micro-structuring processes such as proton-beam writing [7, 8]. More recently, in the growing field of proton radiotherapy [9, 10], PMMA has been used as a material for phantoms and beam-monitoring devices [11]. Therefore, the interaction of various forms of radiation with PMMA has been a persistent topic of

R. S. Thomaz · R. M. Papaléo (✉)
School of Sciences, Pontifical Catholic University of Rio Grande do Sul, Av. Ipiranga 6681, Porto Alegre, RS 90619-900, Brazil
e-mail: papaleo@pucrs.br

V. Kumar et al. (eds.), *Radiation Effects in Polymeric Materials*, Springer Series on Polymer and Composite Materials, https://doi.org/10.1007/978-3-030-05770-1_4

investigation for more than four decades [3, 12–14]. A deep understanding of the radiation effects in PMMA is important not only to evaluate the stability and behavior of this material under various high-energy radiation fields, but also to optimize procedures in modern ion-beam-based processing techniques, where PMMA plays an important role [5–8, 15].

In this chapter, we review fundamental issues related to damaging processes of PMMA films induced by high-energy ions with kinetic energies from a few keV to a few GeV, covering the regimes of energy deposition dominated by either nuclear collisions or electronic excitation. Emphasis is given to present an overview of the bond-breaking processes and the corresponding changes in macroscopic physical properties, and their dependence on the energy loss of the ions.

2 Chemical Modification of PMMA by High-Energy Ions

Polymer degradation encompasses many reactions that change the material's structure, such as irreversible cleavage of bonds in the main chain, intermolecular crosslinking, and formation of unsaturated bonds and of volatile products [16–18]. Both crosslinking and scission may occur simultaneously during irradiation of polymers, but the relative magnitude of crosslinking to scission events depends on the structure of the polymer [1], on the ion stopping power, and ion fluence [19, 20]. In this section, we review the degradation pathways of PMMA by high-energy ions, starting with a discussion of the balance between scission and crosslinking and how it is affected by the stopping power, dE/dx. We then review the radiolysis of PMMA, the main degradation compounds formed, and the structure of highly irradiated PMMA.

2.1 Chain Scission and Crosslinking

The chemical structure of the poly(methyl methacrylate) (PMMA) repeating unit is shown in Fig. 1. For the majority of irradiation conditions, ion-bombarded PMMA

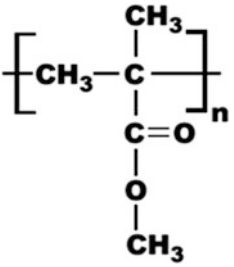

Fig. 1 Chemical structure of the repeating unit of PMMA

undergoes main chain scission, which leads to a decrease of the average molecular weight [19, 21–24]. Chain scission is also dominant in the irradiation of PMMA with γ-rays, electrons, and UV photons [25–27]. The propensity of degradation has been attributed to a steric hindrance due to the methyl ester (CH_3OOC–) groups attached to the PMMA backbone structure [19, 28]. Large pendant groups restrict chain mobility and thus hamper crosslinking. The presence of a tetra-substituted carbon atom in the main chain also favors degradation [29, 30].

Figure 2 shows the molecular weight distribution extracted from PMMA films irradiated with 200 keV He^+ [31]. Even at low fluences (2.5×10^{12} ions/cm^2), the molecular weight distribution (MWD) of bombarded PMMA exhibits a pronounced tail at the low-mass side due to scission products. For higher fluences, the MWD continues to shift toward lower molar masses, but a small fraction of high molecular weight crosslinked molecules is also seen (Fig. 2a).

The solubility of irradiated PMMA increases with fluence (because of chain scission) only until a certain maximum dose (Fig. 2b). For larger fluences, solubility decreases progressively until an insoluble gel is eventually formed. Thus, even for an easily degradable polymer as PMMA, crosslinking of the chains will be extensive at large fluences. The change to a crosslinking dominant behavior occurs in the first place due to the higher concentration of macroradicals at high fluences, which favors bonding in between chains. In addition, at high fluences, PMMA is transformed to a material resembling a sort of disordered polyethylene [32], a polymer for which the probability for crosslinking is higher than for scission [21]. In general, the larger the dE/dx or LET of the ion beam, the lower is the fluence required for the onset of crosslinking in irradiated PMMA. Table 1 illustrates this for beams of H, He, and O ions of 1.5 MeV. The ability of PMMA to crosslink at

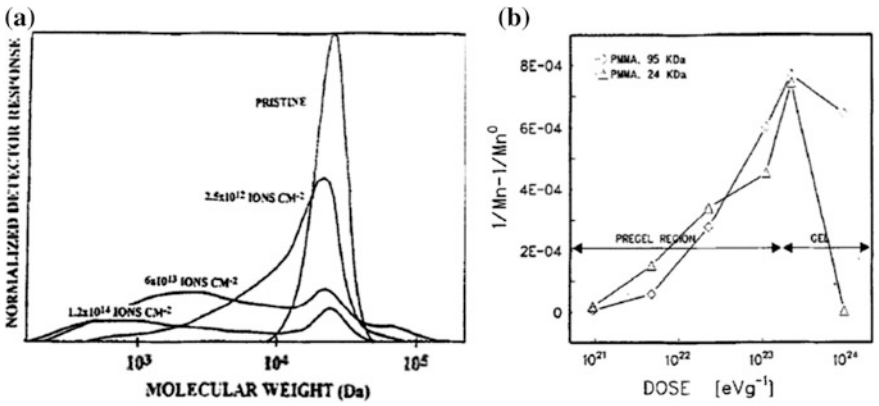

Fig. 2 **a** Molecular weight distribution of 24 kDa PMMA irradiated with 200 keV He^+. **b** $\left(1/M_n - 1/M_n^0\right)$ as a function of dose for samples of 95 and 24 kDa PMMA irradiated with 200 keV He^+. A fluence of 6×10^{13} ions/cm^2 of 200 keV He^+ corresponds to a dose of ~23 eV/g. M_n is the number-averaged molecular weight. Adapted from Ref. [31]

Table 1 Regions of dominance of scission and crosslinking for ion beams of various LET values

Radiation source	LET (eV/nm)	Scission regime (solubility increases with fluence)	Crosslink regime (solubility decreases with fluence)
20 keV e^-	2	$<10^{18}$ m^{-2}	No decrease in solubility
1.5 MeV H^+	20	$<10^{17}$ m^{-2}	$>10^{19}$ m^{-2}
1.5 MeV He^+	200	$<10^{16}$ m^{-2}	$>10^{18}$ m^{-2}
1.5 MeV O^+	800	$<10^{16}$ m^{-2}	$>10^{17}$ m^{-2}

Reprinted with permission from [19] by Publisher

high doses is also seen in electron beam irradiated PMMA, which changes from positive to negative resist behavior (insoluble in the developer) at sufficiently large exposures to the e-beam [33].

Several studies have been conducted to investigate the effect of dE/dx on the yield of chain scission and crosslinking [19, 22, 24]. This is usually quantified by the respective G-values (the number of crosslinks $G(x)$ or chain scissions $G(s)$ per 100 eV of absorbed energy). For irradiation with ^{60}Co gamma rays (dE/dx = 0.2 eV/nm), for example, $G(s) \sim 1.2$ [24]. Similar $G(s)$ values were observed for low LET ion beams (Fig. 3). However, $G(s)$ starts to decrease for beams with LET larger than about 15 eV/nm [19, 22]. $G(s)$ values as low as 0.3 was found at LET = 577 eV/nm (90 MeV O^{4+}) [24]. The lower yield of scission at high LET were attributed to the reduced distance between radical pairs or dangling bonds, which increases the probability for two neighboring radicals to be close enough for crosslinking.

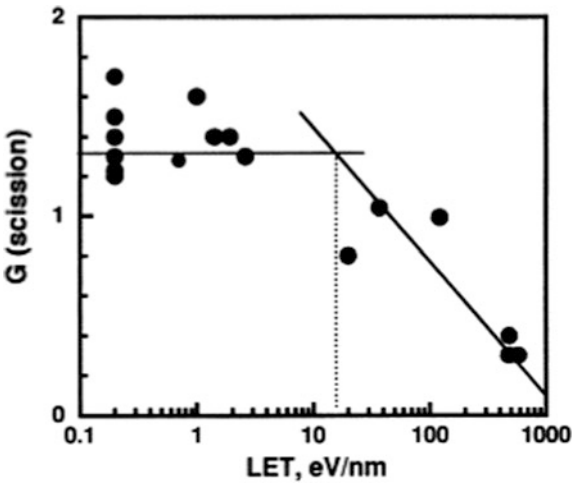

Fig. 3 G-value of chain scission, $G(s)$, for PMMA as a function of LET. Irradiations were performed with different ions and velocities. Reprinted with permission from [19]

An interesting effect related to the degradation of PMMA is ion-beam-induced depolymerization (unzipping) [34]. Unzipping is the main mechanism of thermal degradation of PMMA [35] and is characterized by sequential scissioning of the chain ends, resulting in the preferential emission of the monomer methyl methacrylate [36]. The monomer is found to be the most abundant product (yield > 85%) in the pyrolysis of PMMA [21]. This phenomenon starts at the so-called ceiling temperature (around 220 °C) [34] in the conventional thermal degradation of PMMA. However, when the polymer was exposed to a beam of 200 keV He^+ while heated, unzipping initiated at temperatures as low as 105 °C, slightly above the glass transition temperature (T_g) [34, 37–40]. Thus, irradiation of PMMA at temperatures above T_g may result in a stronger degradation rate and a pronounced reduction in the polymer molecular weight. Up to now, irradiation-induced depolymerization of PMMA has not been detected at room temperature, or using swift heavy ions.

2.2 *Radiolysis, Volatiles, and Changes in the Chemical Structure*

The radiolytic decomposition mechanisms of ion-beam-irradiated PMMA have been extensively investigated, using beams in a wide range of energies and stopping powers [19, 40–42]. While several details have yet to be clarified, especially at the very large dE/dx of swift heavy ions, the general degradation scheme has been established and is not very different from those obtained from "conventional" forms of radiation such as X-rays, electrons, and γ-rays.

A simplified scheme of the mechanism of PMMA degradation is shown in Fig. 4. High-energy irradiation is very efficient for inducing backbone chain scission (Fig. 4-path II) compared to photoexcitation process (path I). Both processes can provoke hydrogen abstraction from the polymer main chain (Fig. 4-path VI) and main chain scission (Fig. 4-path III). Besides main chain scission (and the consequent formation of unsaturated bonds), rupture and decomposition of the side-chain methyl ester groups $CH_3COO–$ are the dominant events (Fig. 4-path IV–V). The main volatiles formed from the decomposition of the pendent group are CO, CO_2, and CH_4 [19, 32, 40, 43]. The amount of such gases will vary depending on the stability of the fragments generated, and on the type of beam.

Figure 5 shows the G-values for CO, H_2, CO_2, and CH_4 production as a function of the track average LET. Again, at low LET, the G-values for ion beams are similar to gamma rays. The G-values start to increase strongly with LET above a LET around 10 eV/nm. Since most of the analyzed gases have the same precursor ($\cdot COOCH_3$), the data of Fig. 5 indicate that the amount of the methyl ester radical must increase with LET [44]. Studies of PMMA irradiated with gamma rays show that the amount of CO, CO_2, and CH_4 are also temperature-dependent [44]. CO and CO_2 yields at T = 40 °C are 2.5–3 times larger than the values found at room

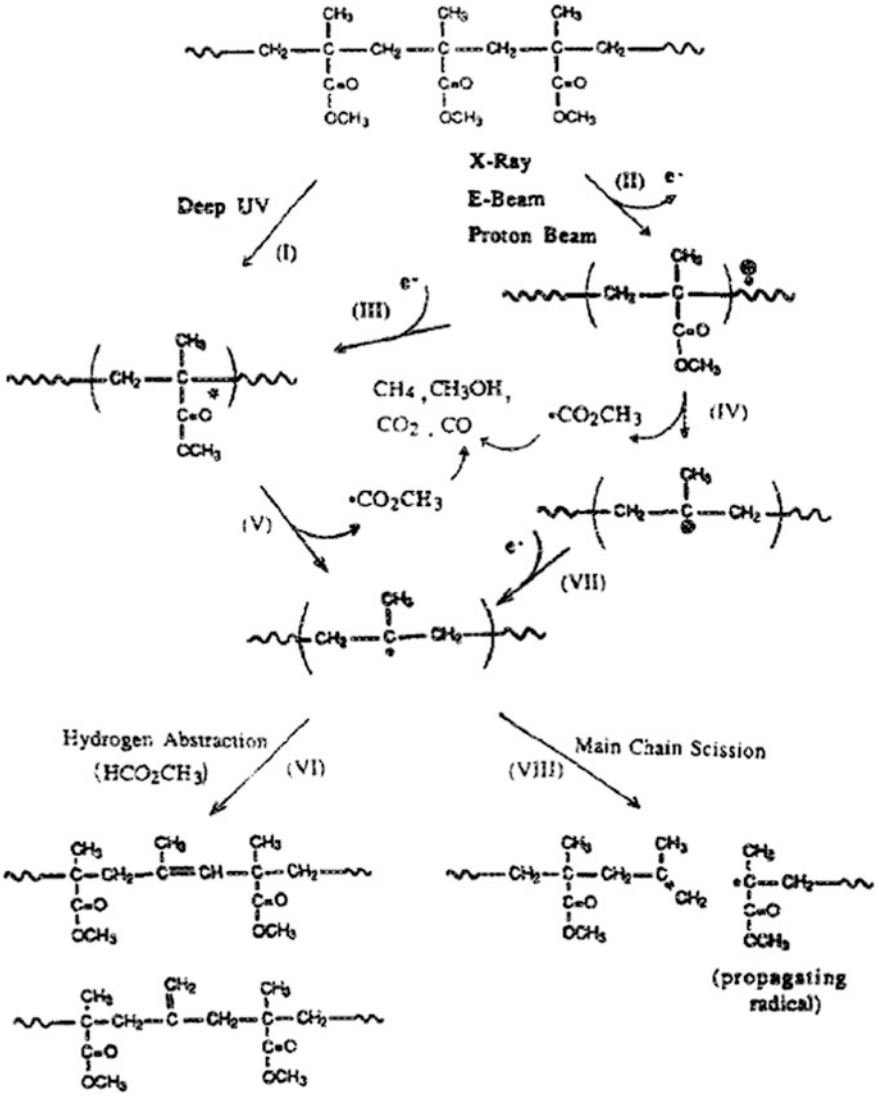

Fig. 4 Radiolysis pathway of PMMA and main volatile products formed. Reprinted with permission from [40]

temperature. On the other hand, molecular hydrogen is produced from radicals that are not thermally dependent.

Many other small molecules originating from the breakage of the chains or from the subsequent decomposition of intermediate species are usually observed by in situ mass spectrometry. Figure 6 shows an example of an in situ residual gas analysis (RGA) of a PMMA film irradiated by 4.5 MeV/u Au ions [45], illustrating

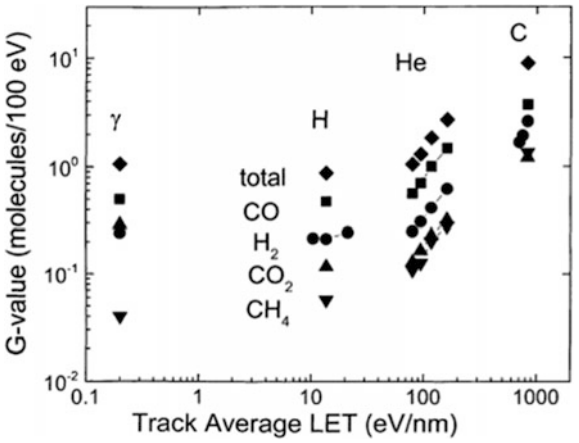

Fig. 5 *G*-values for the production of various volatile molecules as a function of track average LET for beams of γ-rays, H, He, and C ions. Reprinted with permission from [44]

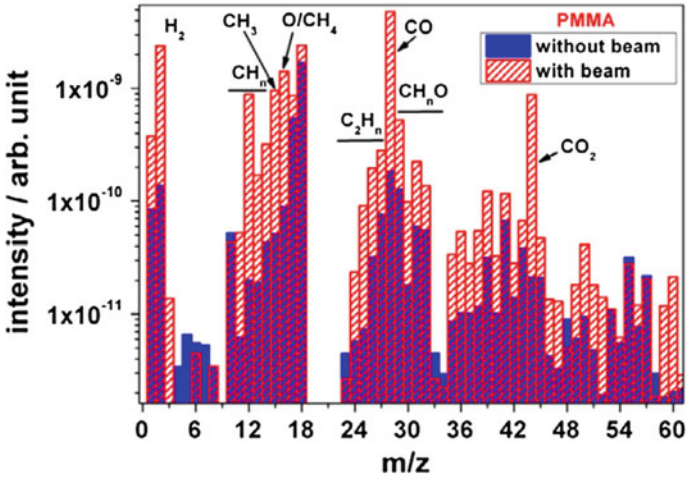

Fig. 6 Outgassing spectra of PMMA irradiated with 4.5 MeV/u Au ions. Mass spectra recorded before and after irradiation. Reprinted with permission from [45]

the multiplicity of emitted species. This includes H_2, CH_2, CH_3, CH_3O•, $HCOOCH_3$, and unsaturated hydrocarbons, such as $H_2C{=}CH_2$, ·$CH{=}C{=}CH_2$, $CH_2{=}C{=}CH_2$, and $CH_3CH{=}CH$ [40, 45, 46]. The abundant emission of oxygen-containing small molecules is a clear indication that a significant fraction of methyl ester groups is broken and easily eliminated by outgassing. The emission of numerous unsaturated hydrocarbons supports the observation of significant scissioning of the macromolecular chains [26, 32].

The decomposition scheme described above is also supported by several spectroscopic studies [20, 31, 32, 40, 47–50]. In particular, infrared vibrational spectroscopy (FTIR) was widely used to probe bond breaking of irradiated PMMA. An example is given in Fig. 7, where FTIR spectra of PMMA bombarded by ions of low (500 keV He) and high dE/dx ($\sim$886 MeV Au) are shown. The reduction of the peaks associated to the vibrational modes at 1150 and 1190 cm^{-1} (C–O stretching vibrations) and the carbonyl (C=O) band at 1720 cm^{-1} are consistent with the gradual elimination of the pendent methyl ester groups (Fig. 7) [20, 26, 47, 48, 51]. The diminishing of carbon–oxygen bonds (C=O and C–O–C) is also shown in the XPS spectra of irradiated PMMA [27, 32, 52, 53] or in measurements of the fraction of oxygen atoms derived from RBS data [26] (Figs. 8 and 9). It is interesting to note that the ratio of oxygen to carbon in a sample irradiated with a beam of low dE/dx ions (2 MeV H$^+$, dE/dx $\sim$ 0.019 keV/nm) is smaller by $\sim$20% than

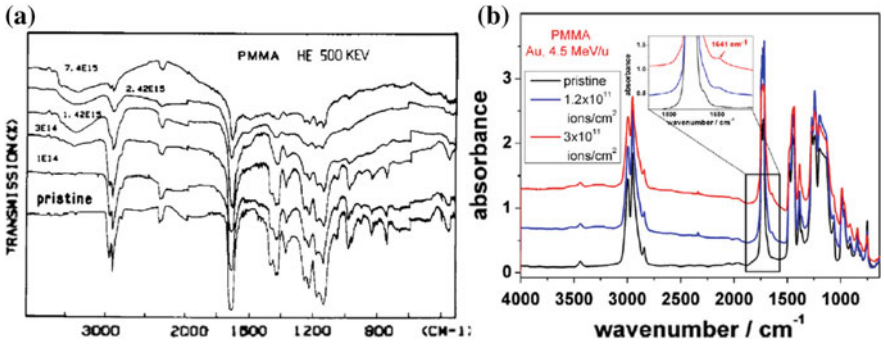

Fig. 7 FTIR spectra of PMMA films bombarded by **a** 500 keV He and **b** 886 MeV Au ions. Reprinted with permission from [45, 54]

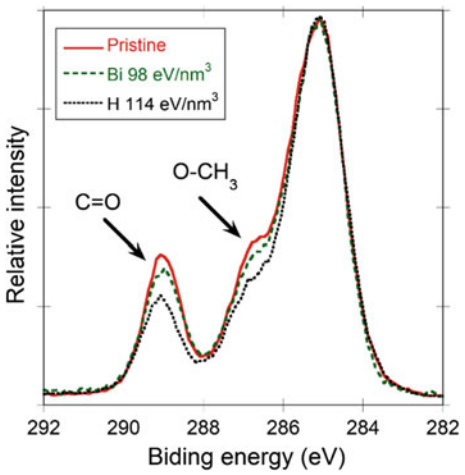

Fig. 8 C1s XPS spectra of PMMA films irradiated by 2 MeV H$^+$ and 2.1 GeV Bi at similar deposited energy densities. The peaks associated to C atoms directly bound to oxygen are labeled in the figure. These are C_3 (O–CH_3) and C_4 (C=O). All spectra were normalized to the peak intensity of the C_1 line (C–H) at 285 eV. Reprinted with permission from [52]

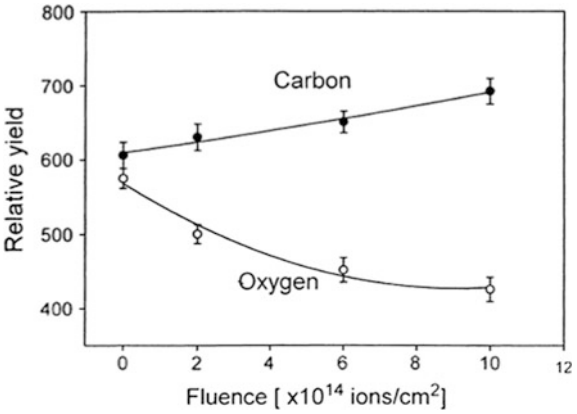

Fig. 9 Change of the relative contents of carbon and oxygen of PMMA irradiated by 350 keV H as a function of fluence, measured by Rutherford backscattering spectrometry. Reprinted with permission from [26]

in a film irradiated with a high dE/dx ion (2.2 GeV Bi, dE/dx $\sim$ 14 keV/nm) at a similar dose (in the case of Fig. 8 close to 100 eV/nm^3) [52]. This suggests a greater importance of particle ejection unzipping by PMMA chains at high dE/dx, which would keep the O/C ratio closer to the pristine value.

FTIR [45, 47, 49], Raman [27], and UV spectroscopy [45, 49] reveal the formation of conjugated C=C bonds in the irradiated polymer. In FTIR, this is seen by the appearance of a new absorption band at 1600–1670 cm^{-1}. In one study, the number of C=C bonds generated in the films was similar to that of C=O groups removed by the same incident dose, suggesting that removal of an ester group generates also a C=C bond by main chain scission and H abstraction [40]. For low dE/dx, the efficiency of C=C bond formation is smaller than that found at high dE/dx (Fig. 7).

At high irradiation fluences, the pristine polymer chemical structure is virtually lost and FTIR spectra are almost featureless due to generalized bond breaking [21, 31, 32, 47, 49]. Carbonization is the fate of all heavily irradiated polymers, but the type of carbonaceous material that is eventually formed depends on the monomer structure and dE/dx of the ions. Most of the studies indicate that PMMA films eventually turn into a form of hydrogenated amorphous carbon material a-C:H [27, 49]. The Raman spectra of PMMA irradiated by 400 keV Cr^+ ions (Fig. 10) show clearly the development of the characteristics broad peaks corresponding to the D and G band of disordered carbon.

Although the general scheme presented above for the radiolysis of PMMA is observed for irradiations with ions in a wide range of stopping powers, there are some effects that are only observed at very high dE/dx due to swift heavy ions. For example, GeV heavy ion irradiation of PMMA leads to the formation of various aromatic compounds [56, 57], including large mass pure carbon clusters [58] that are not observed at low dE/dx [51]. It was suggested that in the core of swift heavy ion tracks, as a result of the very high transient temperatures a gas of electrons and free carbon ions is formed. Carbon clusters and aromatic rings would form during the subsequent expansion and cooling of this highly excited region [58]. The proposed scheme is shown in Fig. 11.

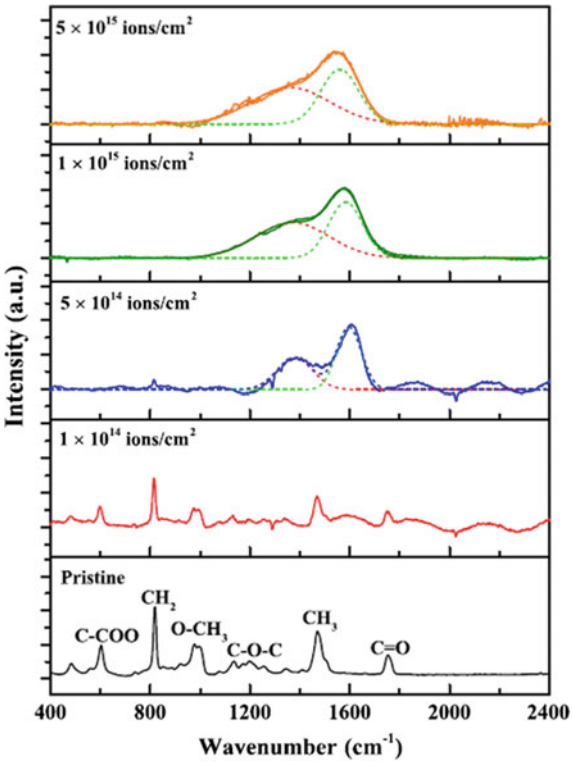

Fig. 10 Raman spectra of pristine and irradiated PMMA samples. The irradiation was performed using 400 keV Cr^+ ions with fluences up to 5×10^{15} cm^{-2}. The solid lines indicate the measured Raman spectrum, while the dashed lines indicate the two Gaussian-fitted D and G bands. Reprinted with permission from [55]

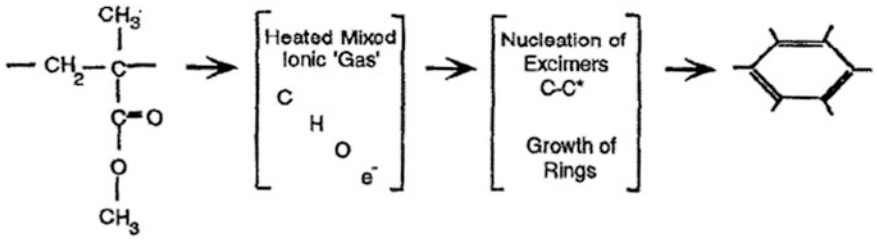

Fig. 11 Suggested mechanisms for the decomposition of PMMA and carbon cluster formation in the core of swift heavy ion tracks. Reprinted with permission from [58]

2.3 Damage Cross Sections

In the previous section, the changes introduced in the chemical structure of irradiated PMMA were reviewed. Here, we discuss the problem of the degradation efficiency and the rates of destruction (or formation) of various chemical bonds. The damaging efficiency is usually quantified extracting the damage cross section σ for a certain process of interest. σ is a probability of occurrence, which is interpreted as an effective area around the ion path where a certain modification takes place. For the quasi-continuous cylindrical damage track of a swift heavy ion, the geometrical interpretation of σ is intuitive. The value of σ can be obtained by monitoring the changes in the intensity $I(\phi)$ of a given signal (a FTIR band, UV absorbance, XRD peaks, etc.) as a function of fluence. In most of the situations, an exponential behavior is observed experimentally, which allows the extraction of a damage cross section by fitting the data with the expression:

$$I(\phi) = I_0 \mathrm{e}^{-\sigma\phi} \tag{1}$$

where I_0 is the intensity of the investigated signal for the pristine sample. If radiation induces the creation of new structures, then the signal intensity can usually be expressed as:

$$I(\phi) = I_{\mathrm{sat}}\left(1 - \mathrm{e}^{-\sigma\phi}\right), \tag{2}$$

where I_{sat} is the signal obtained at high fluences.

Table 2 provides a compilation of cross-sectional values obtained from the literature. Some of them were already extracted in the original references, while others were obtained by us from fittings of the available data. Cross sections for the processes of chain scission, loss of various functional groups, decrease in oxygen and hydrogen content, and formation of conjugated double bonds (chromophores) are shown. The magnitude of the cross sections depends on the technique used to probe the damage (e.g., chemical composition, optical properties, secondary yields) [59], and on the dE/dx and ion velocity. Hence, a direct comparison between cross sections of different processes is only meaningful when similar irradiation conditions are used in the experiments. Despite the large amount of papers on ion beam modification of PMMA, there is, unfortunately, no systematic study comparing cross sections of different processes under similar irradiation conditions, similar to those found, for example, for PET [60], PPS [61], or PC [62]. Yet, some general considerations can be drawn.

The largest damage cross-sectional values are found for processes related to changes in the polymer crystallinity and average molecular weight [60]. For these processes, either the activation energies or the required number of hits by secondary electrons to induce an observable effect is small. However, PMMA is usually in an amorphous configuration (or semi-crystalline structure with high amorphous content). Hence, there are only few studies investigating the changes induced in the

Table 2 Ion energy, velocity, electronic stopping power $(dE/dX)_e$, nuclear stopping power $(dE/dX)_n$, and cross sections (σ) extracted from ion bombardment of PMMA films

Ion	Energy (MeV)	Velocity (cm/ns)	$(dE/dX)_e$ (eV/nm)	$(dE/dX)_n$ (eV/nm)	Technique	σ (cm^2)	Refs.
Bond breaking							
He	5	1.6	1.7	0.0027	FTIR[a,b]	5.1×10^{-16}	Fink [20]
Li	5	1.2	3.3	0.0014	FTIR[a,b]	2.2×10^{-15}	Fink [20]
B	2.5	0.7	5.9	0.1	FTIR[a,b]	2.2×10^{-14}	Fink [20]
H^+	2	1.2	19	0.012	XPS (C–O)	$\sim 4 \times 10^{-16}$	Thomaz [66]
Ar^+	0.005	0.01	69	432	XPS[a] (C–O)	4.1×10^{-15}	Pignataro [32]
He^+	0.2	0.3	200	1	MWD	9×10^{-14}	Fragala [21]
He^+	0.2	0.3	200	1	MWD	3×10^{-13}	Licciardello [64]
He^+	1.0	0.7	250	0.7	Carbon erosion[a]	6×10^{-16}	Calcagno [68]
He^{2+}	0.5	0.5	270	0.6	Dehydrogenation	2.6×10^{-15}	Davenas [49]
Xe^+	0.7	0.1	580	1220	Dehydrogenation	$\sim 10^{-15}$	Davenas [54]
Bi^{+eq}	2200	4.5	14,000	14.4	XPS (C–O)	$\sim 3 \times 10^{-13}$	Thomaz [66]
Au^{eq+}	887.0	2.9	15,000	35	FTIR[a] (2994 cm^{-1})	1.5×10^{-12}	Hossain [45]
Au^{eq+}	887.0	2.9	15,000	35	FTIR[a] (2842 cm^{-1})	9.2×10^{-13}	Hossain [45]
Formation of new bonds							
C^{5+}	70.0	3.3	300	0.2	UV–Vis[a,c]	9.6×10^{-14}	Singh [50]
Ne^{6+}	145.0	3.7	690	0.4	UV–Vis[a,c]	5.5×10^{-13}	Kumar [69]
Si^{8+}	100.0	2.6	1730	1.3	UV–Vis[a,c]	5.6×10^{-13}	Kumar [65]
Au^{eq+}	887.0	2.9	15,000	35	FTIR (1641 cm^{-1})[a]	1.3×10^{-11}	Hossain [45]
U^{eq+}	1980.0	4.0	18,000	21	UV–Vis[a,c]	2.5×10^{-11}	Hossain [45]

[a]The cross sections were extracted from the data presented in the referred references
[b]Data extracted from the whole FTIR spectra
[c]Data extracted from the absorption in 375 nm of the UV–Vis spectra

PMMA crystallinity and cross sections were not extracted [50, 63]. The rates of amorphization nevertheless appear to be similar to those found for molecular weight changes described below. Fragalà et al. [21] investigated the number-averaged molecular weight M_n of PMMA irradiated by 200 keV He^+. Figure 12 shows the values of $1/M_n$ as a function of fluence. The fitting (dashed line) gives a cross section of 9×10^{-14} cm^2. In another study, also with 200 keV He bombardment, a cross section of $\sim 3 \times 10^{-13}$ cm^2 was extracted [64]. The major difference between those two measurements was the procedure used to quantify the signal. While in Ref. [64] only the low-mass portion of the MWD chromatogram was used; Fragalà

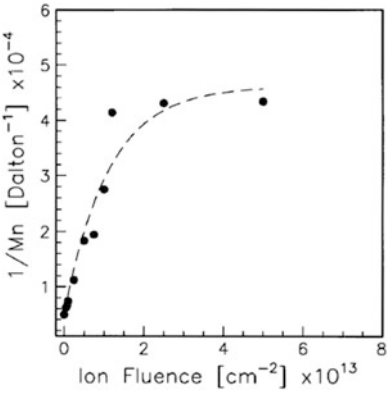

Fig. 12 Reciprocal number-averaged molecular weight $(1/M_n)$ of bombarded PMMA as a function of ion fluence. Reprinted with permission from [21]

et al. [21] used the average over the complete molecular weight distribution. This example illustrates how easily cross sections may be influenced by the procedure of data quantification. In any case, both cross sections are relatively large, considering the low stopping power of the He beam. We found no study on damage cross sections for chain scission of PMMA using swift heavy ions in the literature to compare with.

Cross sections for bond breaking and formation of new bonds in irradiated PMMA are the most abundant in the literature. They typically range from $\sim 10^{-16}$ cm^2 for light ions up to $\sim 10^{-11}$ cm^2 for swift heavy ion projectiles (see Table 2). By monitoring the changes in the intensity of the FTIR bands of PMMA irradiated with MeV light ions (5 MeV He and Li and 2.5 MeV B), Fink et al. [20] found damage cross section of the order of 10^{-16}–10^{-14} cm^2). This corresponds to effective track radii of chemical damage of about 0.4 Å for He or 3 Å for B. On the other hand, the damage cross section of 887 MeV Au ions is roughly three orders of magnitude larger [45]. Figure 13 shows the evolution of three different FTIR bands at 2994, 2842, and 1641 cm^{-1} of PMMA irradiated with 887 MeV Au ions. Both

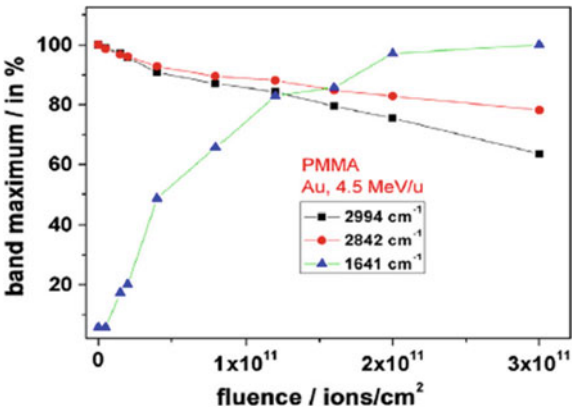

Fig. 13 Peak intensity of absorption bands at 2994, 2842, and 1641 cm^{-1} as a function of the fluence for PMMA films irradiated with 887 MeV Au ions. Reprinted with permission from [45]

processes of bond destruction and new bond formation are shown. The loss of CH_2 and CH_3 groups (bands at 2994 and 2842 cm^{-1}, respectively) occurs with a cross section of $\sigma_{2842\,cm^{-1}} = 7.8 \times 10^{-13}\,cm^2$ and $\sigma_{2994\,cm^{-1}} = 1.5 \times 10^{-12}\,cm^2$. The very large cross section obtained for the new band appearing at 1641 cm^{-1} ($\sigma_{1641\,cm^{-1}} = 1.3 \times 10^{-11}\,cm^2$) demonstrates the efficiency of such high dE/dx ions to create carbon–carbon double bonds, which was larger than the breaking of C–H bonds.

Another process investigated is chromophore formation by the conjugation of unsaturated carbon bonds. This is usually extracted from UV–Vis spectra, as shown in Fig. 14. The absorbance of irradiated samples in the UVA and visible region increases with irradiation fluence. Figure 14b shows the increase in absorbance at 375 nm after irradiation with 100 MeV Si^{8+} ions, depicting an exponential growth typical of Eq. 2. The resulting cross section was about 5.5×10^{-13} cm^2.

Overall, the various damage cross sections extracted for PMMA are comparable to those observed in other polymers, with differences in magnitude that stem from the degree of radiation stability of each material. For example, cross sections for emission of volatiles in polystyrene (a more radiation-resistant polymer) bombarded by 500 keV He, were more than 50% smaller than in PMMA, under the same experimental conditions [49]. On the other hand, heteroatom emission in ion-bombarded PVC, a highly degradable polymer, is even larger than those found for PMMA [66].

Although cross sections are important parameters quantifying the sensitivity of a polymer to radiation damage, care must be taken when comparing data probed by different techniques, because of their specific spatial sensitivity and probing signal. XPS, for example, tends to give smaller cross sections than FTIR, although both techniques are probing the amount of chemical bonds. This is related to the fact that XPS is very little affected by long-range changes in the chemical environment and gives information of modification occurring mostly close to the ion path where

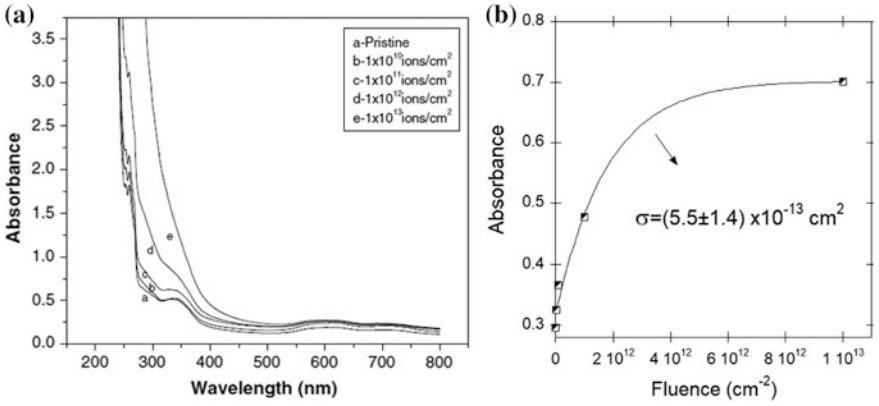

Fig. 14 **a** Optical absorption spectra of pristine PMMA and PMMA after irradiation with 100 MeV Si^{8+} ion beam. **b** Peak intensity of absorption at 375 nm of the spectra shown in (**a**) and its resulting damage cross section. Reprinted with permission from [65]

bond disruption is severe. In addition, the signal from spectroscopic techniques such as UV–Vis and FTIR are proportional to the optical path of the probing beam in the sample. This means that the signal may change not only because specific bonds are broken, but also due to reductions in the sample thickness. As discussed in the next section, PMMA thinning by ion irradiation is very efficient [67]. Therefore, many of the cross sections reported in the literature may be the convolution of chemical damage with effects that cause thickness reductions (sputtering, densification, etc.).

2.4 Changes in Physicochemical Properties

Bond breaking, formation of new bonds, and preferential emission of oxygen and hydrogen in bombarded PMMA result in irreversible changes in its macroscopic physicochemical properties. In this section, the main changes observed in mechanical, optical, and electrical properties of ion-bombarded PMMA are reviewed.

2.4.1 Density Enhancement and Compaction

PMMA films and foils irradiated by ion beams become remarkably thinner after ion bombardment [26, 43, 70–72]. The thickness decrease was mainly attributed to outgassing of volatile products [73, 74]. Sputtering is a small component, especially for light ions and low dE/dx, but cannot be neglected for swift heavy ions. The crater volume of a single 600 MeV Au ion is approximately a half sphere of 10 nm radius [75, 76]. In addition, main chain scission results in shorter and more mobile molecules, what facilitate spatial rearrangements and local conformational changes. This eventually leads to the compaction of the layers and increase in density [77, 78].

Figure 15 presents the compaction induced in 1-mm-thick PMMA foils irradiated with 350 keV H^+ (the ion range is 4.2 μm) as a function of the fluence. The compaction reached values as high as few micrometers at high fluences. The shrinking rate was not steady, but decreased with fluence, until a saturation level is reached at very high fluences [67, 71, 78]. This occurs because of the cumulative effects of track overlap. At large fluences, the probability of ions hitting regions already modified by the ions increases, reducing the gas yield per ion impact.

Swelling, however, may precede the shrinking process. Due to the long projected range of swift ions, gaseous products are formed in deep regions of the polymer and cannot escape from the material as quick as they are produced. As a consequence, a high pressure of gases is built up in the polymer, resulting in a transiently swollen surface [74]. In a foil of PMMA irradiated through a micro-patterned mask with 1.8 MeV H^+ ($\phi = 6 \times 10^{13}$ ions/cm^2), within a time of 12 min after the irradiation the surface swollen about 70 nm with respect to the non-irradiated region (Fig. 16a). Only later, 200 min after the irradiation,

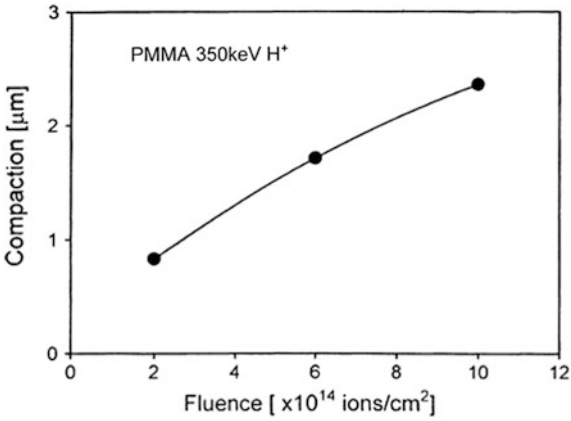

Fig. 15 Compaction of a 1-mm-thick PMMA foil as a function of fluence of 350 keV H^+ ions. Reprinted with permission from [26]

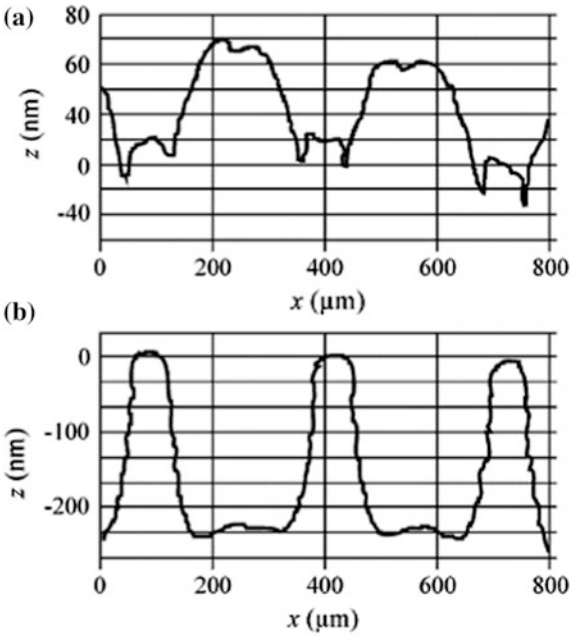

Fig. 16 Surface profiles of the irradiated sample measured by profilometry, **a** 12 min after the irradiation and **b** after 200 min. Reprinted with permission from [74]

profilometry of the same region revealed that the surface retracted to more than 200 nm below the original surface level (Fig. 16b). It was noted by the authors that if the ion current was low enough, swelling was not observed.

A discrepancy between compaction values is found in the literature, even when similar irradiation conditions are used [43, 74]. These differences can be explained by the distinct times after irradiation that the depth profile was measured. The shrinking due to outgassing is diffusion-limited and may continue over several

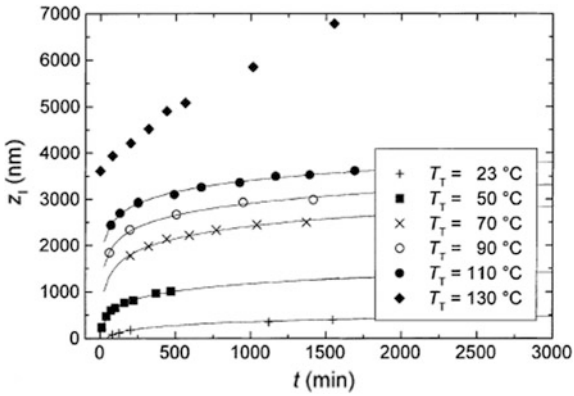

Fig. 17 Shrinking of the surface (z_t) of 1-mm-thick PMMA foils bombarded with 1.8 MeV H^+ ions as a function of time t after irradiation to a fluence of 6×10^{13} ions/cm^2. Measurements were performed at different temperatures T_T ranging from 23 to 130 °C. The solid lines are fittings with a diffusion model. Reprinted with permission from [74] by Publisher

weeks if the effective diffusion coefficient, D_{eff} is low (Fig. 17). At room temperature, the D_{eff} extracted for PMMA after irradiation with 1.8 MeV H^+ ions to a fluence of 6×10^{13} cm^{-2} was 8.3×10^{-11} cm^2/s. Gas diffusion is accelerated at higher temperatures, increasing the shrinking rate. At temperatures just below the glass transition, T_g ($\sim$105 °C), the effective diffusion constant found by Schrempel et al., is about six orders of magnitude higher than the value found at room temperature [74]. At 130 °C, thermal degradation also plays an important role, being gas diffusion no longer the predominant effect.

2.4.2 Optical Properties

There has been a great practical interest on the investigation of optical properties of irradiated PMMA, because of the wide range of potential photonic applications and the widespread use of PMMA in optical components. Proton-beam writing has been used for the fabrication of microphotonic devices (waveguides, gratings, microlens arrays, etc., Fig. 18). For such applications, knowledge on ion-induced modifications in the absorption coefficient and refractive index are of utmost importance.

As discussed in the previous section, the damage produced by ion irradiation leads to the formation of absorption centers in PMMA at the UV and visible regions of the spectra due to the increase in conjugated C=C double bonds, which provides more optically active electrons. This process changes the polymer color gradually from transparent to yellowish-brown. The color change is usually irreversible, but there are reports of transparency recovery depending on the beam conditions and storage environment [28].

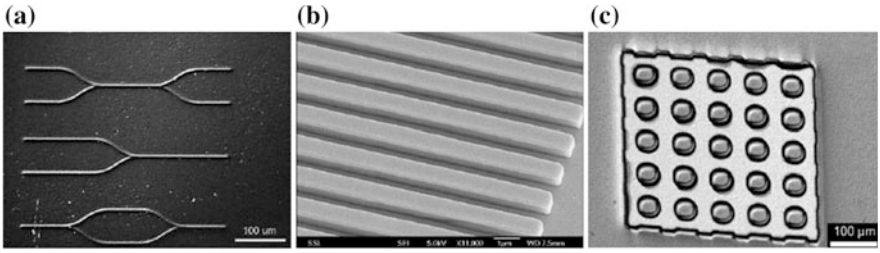

Fig. 18 **a** Optical image of waveguides fabricated in 3-mm-thick PMMA. Electron microscopy images of a **b** surface relief gratings fabricated in 800 nm layer of PMMA spin coated on a Si wafer and **c** a microlens array. Adapted from [79]

Accompanying the changes in UV absorption, there is an increase in the refractive index with ion fluence (Fig. 19) [47, 71, 72, 80, 81]. The refractive index enhancement was attributed as well to the formation of unsaturated bonds along the irradiated layer [28]. Compaction and densification of the irradiated material are also associated to the increase in the refractive index [77]. It is remarkable in the study of Kallweit and Biersack [80] that Δn increases steadily with fluence, with no saturation yet visible (Fig. 20). The relatively large changes in Δn of up to 0.3 is an interesting feature for waveguide fabrication.

Several experiments were performed to investigate the correlation between the ion range and the changes of Δn with depth. When 2 MeV H^+ was used to bombard a block of PMMA (Fig. 21), the highest increase of the refractive index occurs at the end of range, i.e., at the Bragg peak of the energy-loss curve [81].

The use of irradiated PMMA in waveguides was also tested. The main problem was the optical losses. The measured intensity attenuation of waveguides fabricated using a 3-mm-thick foil irradiated by 2 MeV H^+ at fluence of $\sim$50 nC/mm^2 is shown in Fig. 22. In this case, the mean attenuation coefficient was found to be 1.4 $\pm$ 0.2 dB/cm [70]. Propagation losses are, additionally, very dependent on the ion dose [72]. For PMMA blocks irradiated with Li^+ ions in the energy range of 100–130 keV with fluences up to 10^{14} cm^{-2}, waveguides with total loss values of

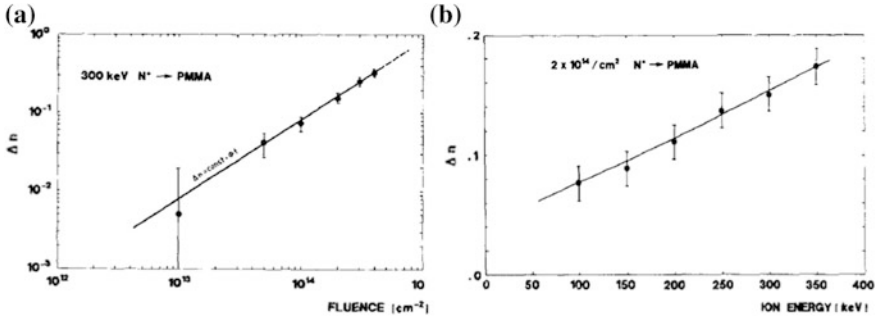

Fig. 19 Change in refractive index, Δn, of PMMA irradiated by N ions with kinetic energies between 100 and 350 keV. **a** Δn versus ion fluence for 300 keV N^+. **b** Δn versus ion energy (constant fluence of 2 $\times$ 10^{14} ions/cm^2). Reprinted with permission from [80]

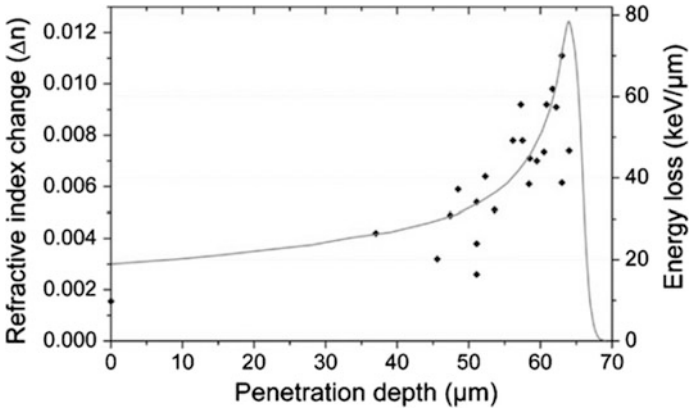

Fig. 20 Change in refractive index at 633 nm of PMMA irradiated by 2 MeV H^+ as a function of penetration depth. For comparison, the energy-loss profile was also plotted as a solid line. Reprinted with permission from [81]

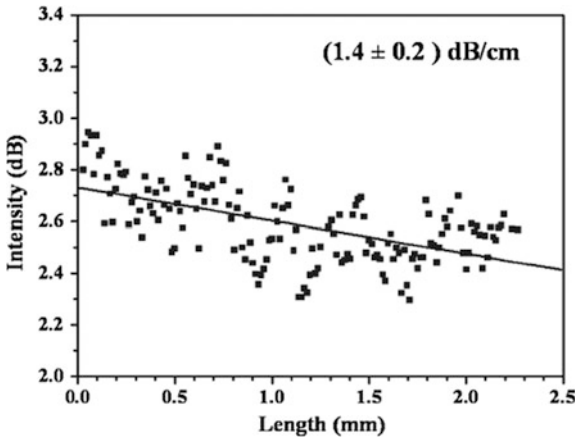

Fig. 21 Intensity loss at 632.8 nm of a PMMA waveguide fabricated using 2 MeV H^+ at fluence of $\sim$50 nC/mm^2. Reprinted with permission from [70]

<2 dB/cm could be fabricated [47]. At higher fluences, because of ion-beam-induced damage, the propagation loss increases by more than a factor of two. Optical losses are also a function of the beam energy. Other studies show that attenuation measurements of waveguides obtained after 1–2 MeV proton irradiation showed loss values as high as 5 dB/cm up to 8 dB/cm, depending on the beam conditions [71].

Another complication of using ion irradiation to prepare waveguides is aging. In one study, long-term stability of n was investigated in PMMA bombarded by 1 MeV He^+ ions and stored at 70 °C in vacuum or at ambient conditions (Fig. 23). Both samples show a decrease of the initial index of refraction during the first 60 days and become stable after 3 months. The aging effect was more pronounced for the samples stored at ambient conditions [71].

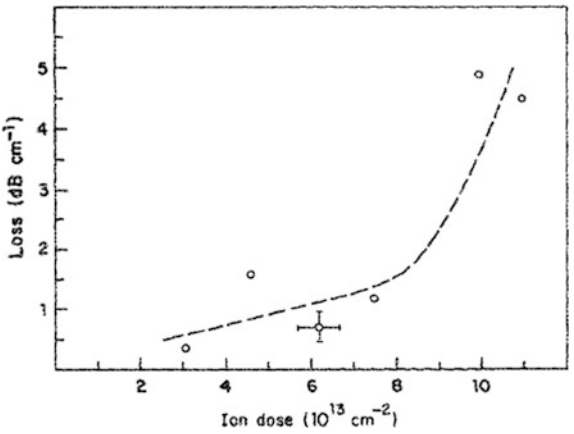

Fig. 22 Loss value of irradiated PMMA waveguides for different fluences of Li^+ ions in the energy range of 100–130 keV. Reprinted with permission from [47]

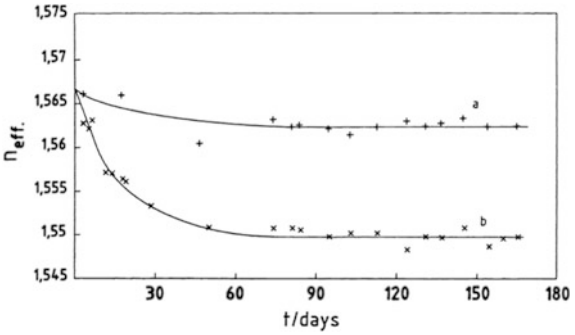

Fig. 23 Long-term stability of the refraction index of PMMA samples irradiated with 1 MeV He^+ ions. Reprinted with permission from [71]

2.4.3 Mechanical Properties

Figure 24 shows the results of the changes of flexural strength of 3-mm-thick sheets of PMMA irradiated by 45 and 30 MeV proton beams and γ-rays as a function of the absorbed dose. The decay in flexural strength is similar for all types of such low LET radiations (LET $\sim$ 1 eV/nm for the three beams). It is well known that such a decrease of the strength is induced by chain scission of PMMA [82].

Hardness, scratch resistance, and elastic modulus of the polymer are also affected by crosslink and chain scission [23, 83]. Figure 25 shows averaged values of indentation elastic modulus versus maximum indentation depth for bulk PMMA implanted by 40 keV B^+ ions. The maximum penetration depth of B^+-ions into PMMA is about 400 nm. However, implanted PMMA showed an increased elastic modulus with respect to the pristine material at much larger depths (up to 1100 nm [84]).

Figure 26 illustrates the changes in hardness of PMMA irradiated by 2 MeV Ar ions (LET = 1134 eV/nm) and 2 MeV He ions (LET = 242 eV/nm) as a function of ion fluence. Hardness increased significantly with increasing fluence, especially

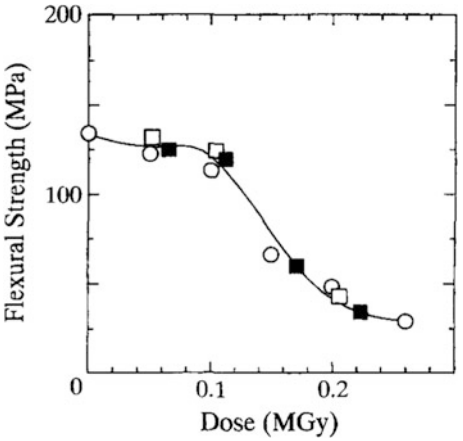

Fig. 24 Flexural strength of PMMA as a function of dose (○ gamma ray; □ 45 MeV proton; ■ 30 MeV proton). Reprinted with permission from [82]

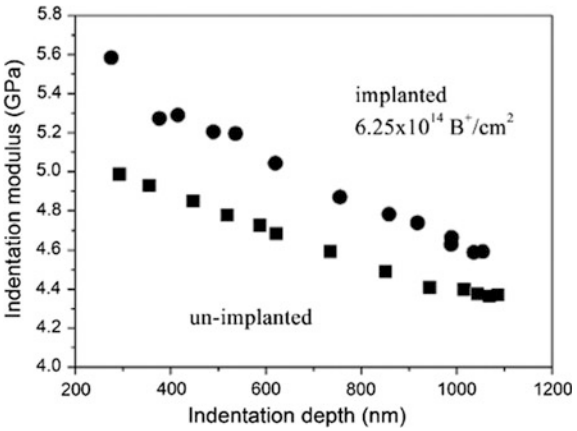

Fig. 25 Indentation elastic modulus versus maximum indentation depth for un-implanted PMMA (squares) and PMMA implanted by 40 keV B^+ ions (circles) samples. Reprinted with permission from [84]

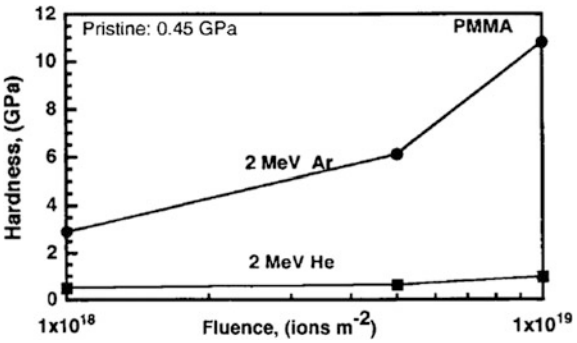

Fig. 26 Hardness changes as a function of fluence for PMMA irradiated by 2 MeV He^+ and Ar^+ ions. Reprinted with permission from [19]

for the larger dE/dx Ar beam, where it jumped from the pristine value of 0.45 GPa to over 10 GPa after irradiation to a fluence of 1×10^{15} cm^{-2}. The improvement in hardness was greater at larger dE/dx [19]. In fact, under low LET radiations, such as e-beam and γ-rays, the material becomes extremely brittle, but there is no appreciable change in hardness [19]. However, it has been shown that at high electron doses (7.5×10^{17} cm^{-2}), the surface hardness of the irradiated PMMA increased to 2.8 GPa, and the elastic modulus from 5.6 to 22.9 GPa [27].

As hardness of polymers increases with increasing crosslinking density [83], this difference in mechanical behavior of PMMA irradiated by ions of low and high LET reinforces that scission is dominant for low LET and low fluences, whereas crosslinking becomes more important with increasing LET and at high ion fluences.

2.4.4 Changes in Electrical Properties

In general, polymers are highly insulating materials with wide band gaps [28]. Ion irradiation or implantation can be used to increase the polymer conductivity by several orders of magnitude. The possibility of preparing conducting regions in a highly insulating polymeric matrix was one of the first exciting effects of ion bombardment of polymers to be explored [85]. Figure 27 presents data on the electrical conductivity of irradiated PMMA as a function of 400 keV Cr^+ ions. An increase in electrical conductivity from $\sim 2 \times 10^{-10}$ S/cm (pristine) to $\sim 7 \times 10^{-6}$ S/cm (at 5×10^{15} ions/cm^2) was observed. In another study, using beams of 150–200 keV Si^+ ions at much larger fluences (3.2×10^{16} Si^+/cm^2), the conductivity reached values of almost 11 orders of magnitude higher than that of pristine PMMA [86].

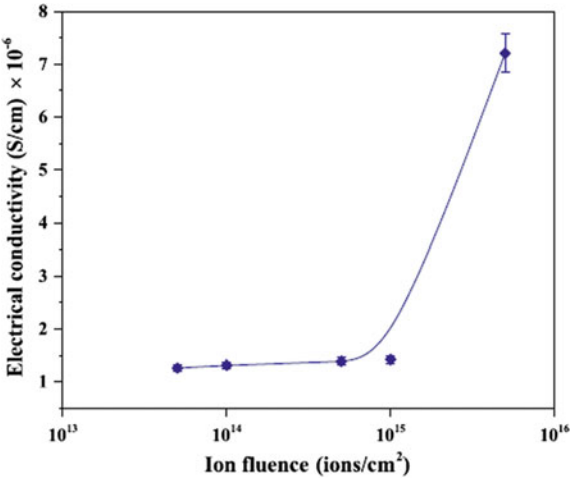

Fig. 27 Electrical conductivity of 400 keV Cr^+-implanted PMMA versus ion fluence. The line was drawn to guide the eye. Reprinted with permission from [55]

The conductivity increase reflects the carbonization process discussed in the previous sections. Conductivity rises sharply only after the material has been extensively damaged by the beam and significant amounts of carbon clusters are formed in the material. The formation of a network of carbon clusters provides a charge transportation system in implanted PMMA [55, 85]. In the early work at the Bell Laboratories [85, 87], 2 MeV Ar^+ was used to irradiate several nonpolymeric and polymeric organic compounds, including PMMA. The temperature dependence of the resistivity $\rho(T)$ of the irradiated material was found to follow $\rho(T) \propto \exp\left[+(T_0/T)^{1/2}\right]$ over a wide range of fluences and temperatures. Based on this dependence, it was proposed that conduction of electricity at intermediate irradiation fluences involves hopping of carriers between isolated conducting islands. At very high fluences, ($>10^{16}$ cm^{-2}), conducting islands interconnect and the resistivity becomes temperature-independent. In general, ion bombardment of organic thin films leads to the production of a carbon-enriched material with some properties similar to those found for amorphous carbon, but with electrical characteristics that are unique [87]. Conductivity also depends on the initial monomer structure. The value found for heavily irradiated PMMA (9.5×10^{-4} S/cm, after 10^{16} ions/cm^2 of 1 MeV Xe^+) was smaller than for other polymers like PS (1×10^{-4} S/cm) and PE (1.5×10^{-4} S/cm) irradiated under similar conditions [54].

3 Concluding Remarks

In this chapter, fundamental issues related to damaging processes of PMMA induced by high-energy ions were reviewed. The different steps in the polymer modification, from the identification of the main bond-breaking pathways and chemical changes to the corresponding modifications in the macroscopic physical properties are reasonably well established, and are not very different from those obtained from "conventional" forms of radiation, for which the available data is much more abundant. The similarities are more evident for low LET particles, such as fast H or He ions. In this regime, *G*-values for X-rays, γ-rays, electrons, and ions are similar and the mean dose is the main parameter determining the level of the final effect (chain scission, hydrogen release, etc.). However, several details of the complex chain of events induced by high-energy ions in PMMA have yet to be clarified, especially at the very large d*E*/d*x* of swift heavy ions (SHI).

In fact, already at intermediate d*E*/d*x* (e.g., of 1 MeV Ar, ~800 eV/nm), the dose/response curve might become nonlinear. Certain degradation products are clearly produced at much higher yields at large d*E*/d*x*. This includes the formation of triple bond carbon clusters, and sputtering of macromolecular fragments. Thus, although carbonization is the fate of all heavily irradiated polymers, the type and properties of the carbonaceous material that is eventually formed will depend on the

dE/dx of the ions. The balance between scission and crosslinking and ion-beam-induced unzipping are also expected to alter at large dE/dx. Systematic studies aiming a better understanding of transformations specifically induced by energetic heavy ions are necessary. Even the basic effect of the changes in M_w distribution of PMMA after SHI irradiation is lacking in the literature. Of the major physical properties of materials, thermal property is one of the least investigated after ion irradiation of polymers, including PMMA. Studies on the changes in thermal properties like thermal expansion or heat conductivity are practically absent in the literature and need to be conducted. There are scattered data on damage cross sections for bond-breaking of PMMA in the literature. However, there is no systematic study comparing cross sections of different modification processes (chain scission, bond breaking, chromophore formation, carbon cluster formation, etc…) under the same irradiation conditions. This will allow a detailed view of the spatial (radial) distribution of different types of structures/defects created around the ion track.

The effect of irradiation temperature is also worthy of further investigation. We have shown examples where temperature alters the effects produced by ion irradiation of PMMA (e.g., in irradiation-induced depolymerization or in the kinetics of volatile emission). However, it is unclear at present how temperature alters the profile of intermediate products produced by ion irradiation or the final properties of the bombarded material. It is expected that, near and above T_g, all processes which are diffusion-controlled will be enhanced. The temperature effects may also be different for ions of high and low dE/dx, as recent studies on the surface morphology of ion-irradiated PMMA thin films suggest [88]. Irradiations at low temperatures with subsequent in situ annealing and spectroscopic characterization will allow obtaining valuable information on the creation and stability of different chemical groups formed by irradiation. This has been explored in a few polymers, like polyethylene, but not in PMMA.

The vast majority of irradiation experiments are performed in vacuum. It would be interesting to study the effect of ion irradiation in different atmospheres, including oxidative environments, and how they affect the yield and type of degradation products.

Additionally, the influence of the sample conditions themselves needs to be carefully addressed. For example, there is no systematic investigation comparing irradiation effects on samples prepared from monodisperse standards in a broad range of molecular weights. How much the molar mass influence radiation chemistry and properties changes induced by energetic ions? PMMA is also used in the form of composites with various fillers or polymer blends. A systematic investigation of the ion beam modification of such systems is also scarce and needs to be examined in closer detail.

Overall, in spite of the importance of PMMA as an engineering material, the volume of data available on ion modification of PMMA is still relatively limited,

compared to other important polymers such as polystyrene, polyethylene, or poly (ethylene terephthalate). Thus, PMMA needs for sure an expanded and reliable database, built from "targeted" experiments with well-controlled irradiation and sample conditions to help answering some of the open issues raised above.

References

1. Duan H, Zhao J, Zhang Y, Xie E, Li H (2009) Nanotechnology 20(13):135306
2. Frazer R, Byron R, Osborne P, West K (2005) J Long Term Effects Med Implants 15:629–639
3. Komuro M, Atoda N, Kawakatsu H (1979) J Electrochem Soc 126(3):483–490
4. Hall TM, Wagner A, Thompson LF (1982) J Appl Phys 53(6):3997–4010
5. Gorelick S, Guzenko VA, Vila-Comamala J, David C (2010) Nanotechnology 21(29):8
6. Vladimirsky Y, Vladimirsky O, Morris KJ, Klopf JM, Calderon GM, Saile V (1996) Microelectron Eng 30(1–4):543–546
7. Puttaraksa N, Norarat R, Laitinen M, Sajavaara T, Singkarat S, Whitlow HJ (2012) Nucl Instrum Methods Phys Res Sect B 272:162–164
8. van Kan JA, Malar P, Wang YH (2014) Appl Surf Sci 310:100–111
9. Schardt D, Elsaesser T, Schulz-Ertner D (2010) Rev Mod Phys 82(1):383–425
10. Loeffler JS, Durante M (2013) Nat Rev Clin Oncol 10(7):411–424
11. Linz U (2011) Ion beam therapy: fundamentals, technology, clinical applications. Springer, Berlin
12. Randall JN, Flanders DC, Economou NP, Donnelly JP, Bromley EI (1983) Appl Phys Lett 42(5):457–459
13. Dole M (2013) The radiation chemistry of macromolecules, vol. 2. Elsevier Science, Netherlands
14. Egusa S, Ishigure K, Tabata Y (1979) Macromolecules 12(5):939–944
15. Trautmann C (2010) Micro- and nanoengineering with ion tracks. In: Ion beams in nanoscience and technology. Springer, Heidelberg, pp 369–387
16. Chapiro A (1995) Nucl Instrum Methods B 105(1–4):5–7
17. Marletta G (1990) Nucl Instrum Methods B 46(1–4):295–305
18. Duraud JP, LeMoel A (1995) Nucl Instrum Methods B 105(1–4):71–80
19. Lee E, Rao G, Mansur L (1999) Radiat Phys Chem 55(3):293–305
20. Fink D, Hosoi F, Omichi H, Sasuga T, Amaral L (1994) Radiat Eff Defects Solids 132(4): 313–328
21. Fragala M, Compagnini G, Licciardello A, Puglisi O (1998) J Polym Sci Pol Phys 36(4):655–664
22. Kudoh H, Sasuga T, Seguchi T (1997) Radiat Phys Chem 50(3):299–302
23. Lee EH (1999) Nucl Instrum Methods B 151(1–4):29–41
24. Schnabel W, Klaumunzer S, Sotobayashi H, Asmussen F, Tabata Y (1984) Macromolecules 17(10):2108–2111
25. Schnabel W, Sotobayashi H (1976) Polym J 8(5):423–427
26. Choi HW, Woo HJ, Hong W, Kim JK, Lee SK, Eum CH (2001) Appl Surf Sci 169:433–437
27. Cho SO, Jun HY (2005) Nucl Instrum Methods B 237(3–4):525–532
28. Fink D (2004) Fundamentals of ion-irradiated polymers. Springer, Berlin
29. Compton RG, Bamford CH, Tipper CFH (1975) Degradation of polymers. Elsevier Science, Netherlands
30. Grassie N, Scott G (1988) Polymer degradation and stabilisation. Cambridge University Press, Cambridge

31. Licciardello A, Fragala M, Foti G, Compagnini G, Puglisi O (1996) Nucl Instrum Methods B 116(1–4):168–172
32. Pignataro B, Fragala M, Puglisi O (1997) Nucl Instrum Methods B 131(1–4):141–148
33. Zailer I, Frost JEF, Chabasseur V, Ford C, Pepper M (1999) Semicond Sci Technol 11:1235
34. Fragala ME, Compagnini G, Torrisi L, Puglisi O (1998) Nucl Instrum Methods B 141(1–4): 169–173
35. Manring LE (1989) Macromolecules 22(6):2673–2677
36. Manring LE (1988) Macromolecules 21(2):528–530
37. Mahoney CM, Fahey AJ, Gillen G, Xu C, Batteas JD (2007) Anal Chem 79(3):837–845
38. Compagnini G, Angilella GGN, Raudino A, Puglisi O (2001) Nucl Instrum Methods B 175:559–563
39. Fragala ME, Compagnini G, Puglisi O (1999) J Mater Res 14(1):228–231
40. Choi JO, Moore JA, Corelli JC, Silverman JP, Bakhru H (1988) J Vac Sci Technol B 6:2286
41. Wochnowski C, Eldin MAS, Metev S (2005) Polym Degrad Stab 89(2):252–264
42. Chang Z, LaVerne JA (2000) J Phys Chem B 104(45):10557–10562
43. Schrempel F, Witthuhn W (1997) Nucl Instrum Methods B 132(3):430–438
44. Chang Z, LaVerne JA (2001) Radiat Phys Chem 62(1):19–24
45. Hossain UH, Lima V, Baake O, Severin D, Bender M, Ensinger W (2014) Nucl Instrum Methods B 326:135–139
46. Ruck DM, Schulz J, Deusch N (1997) Nucl Instrum Methods B 131(1–4):149–158
47. Kulish JR, Franke H, Singh A, Lessard RA, Knystautas EJ (1988) J Appl Phys 63(8):2517–2521
48. Szilasi SZ, Huszank R, Szikra D, Vaczi T, Rajta I, Nagy I (2011) Mater Chem Phys 130(1–2): 702–707
49. Davenas J, Thevenard P, Boiteux G, Fallavier M, Lu XL (1990) Nucl Instrum Methods B 46 (1–4):317–323
50. Singh P, Kumar R, Virk H, Prasad R (2010) Indian J Pure AP Phy 48(5):321–325
51. Fink D, Mockel HJ, Melzer H, Klett R, Cardoso J, Montiel R, Vazquez H, Hosoi F, Omichi H, Wang L, Chadderton LT (1997) Appl Phys A 64(1):61–68
52. Thomaz R, Gutierres LI, Morais J, Louette P, Severin D, Trautmann C, Pireaux JJ, Papaléo RM (2015) Nucl Instrum Methods B 365:578–582
53. Kallweit R, Roll U, Strack H, Pocker A (1992) Mal Res Soc Symp Proc 235:345–350
54. Davenas J, Xu XL, Boiteux G, Sage D (1989) Nucl Instrum Methods B 39(1–4):754–763
55. Arif S, Rafique MS, Saleemi F, Naab F, Toader O, Mahmood A, Aziz U (2016) Appl Phys A 122(9)
56. Fink D, Chadderton LT, Schmoldt A (1993) Nucl Tracks Rad Meas 22(1–4):51–52
57. Schmoldt A, Chadderton LT, Fink D (1994) Radiat Eff Defects Solids 128(4):277–285
58. Fink D, Chadderton L, Hosoi F, Omichi H, Sasuga T, Schmoldt A, Wang L, Klett R, Hillenbrand J (1994) Nucl Instrum Methods B 91(1–4):146–150
59. Papaleo RM (1997) Nucl Instrum Methods B 131(1–4):121–134
60. Papaleo RM, Dearaujo MA, Livi RP (1992) Nucl Instrum Methods B 65(1–4):442–446
61. Papaleo R, Hallen A, Sundqvist B, Farenzena L, Livi R, deAraujo M, Johnson R (1996) Phys Rev B 53(5):2303–2313
62. Sun YM, Zhu ZY, Wang ZG, Jin YF, Liu J, Hou MD, Zhang QX (2003) Nucl Instrum Methods B 209:188–193
63. Singh P, Kumar R, Cyriac J, Rahul MT, Nambissan PMG, Prasad R (2014) Nucl Instrum Methods B 320:64–69
64. Licciardello A, Fragala ME, Compagnini G, Puglisi O (1997) Nucl Instrum Methods Phys Res Sect B-Beam Interact Mater Atoms 122(3):589–593
65. Kumar R, Ali S, Mahur A, Virk H, Singh F, Khan S, Avasthi D, Prasad R (2008) Nucl Instrum Methods B 266(8):1788–1792
66. Thomaz R, Louette P, Hoff G, Müller S, Pireaux JJ, Trautmann C, Papaléo RM (2018) Phys Rev Lett 121(6):066101

67. Unai S, Puttaraksa N, Pussadee N, Singkarat K, Rhodes MW, Whitlow HJ, Singkarat S (2013) Microelectron Eng 102:18–21
68. Calcagno L, Compagnini G, Foti G (1992) Nucl Instrum Methods B 65(1–4):413–422
69. Kumar R, Ali S, Singh P, De U, Virk H, Prasad R (2011) Nucl Instrum Methods B 269 (14):1755–1759
70. Sum TC, Bettiol AA, Florea C, Watt E (2006) J Lightwave Technol 24(10):3803–3809
71. Ruck DM, Brunner S, Frank W, Kulisch J, Franke H (1992) Surf Coat Technol 51(1–3): 318–323
72. Hong W, Woo HJ, Choi HW, Kim YS, Kim GD (2001) Appl Surf Sci 169:428–432
73. Ruck DM (2000) Nucl Instrum Methods B 166:602–609
74. Schrempel F, Kim YS, Witthuhn W (2002) Appl Surf Sci 189(1):102–112
75. Papaleo RM, Silva MR, Leal R, Grande PL, Roth M, Schattat B, Schiwietz G (2008) Phys Rev Lett 101(16):167601
76. Papaleo RM, Thomaz R, Gutierres LI, de Menezes VM, Severin D, Trautmann C, Tramontina D, Bringa EM, Grande PL (2015) Phys Rev Lett 114(11):118302
77. Sum TC, Bettiol AA, Seng HL, Rajta I, van Kan JA, Watt F (2003) Nucl Instrum Methods B 210:266–271
78. Ruck DM, Schulz J, Frank WF (1996) In: Conference on photopolymer device physics, chemistry, and applications III, Proceedings of the society of photo-optical instrumentation engineers (Spie). Denver, Co, pp 118–128
79. Bettiol AA, Sum TC, Cheong FC, Sow CH, Rao SV, van Kan JA, Teo EJ, Ansari K, Watt F (2005) Nucl Instrum Methods B 231:364–371
80. Kallweit R, Biersack JP (1991) Radiat Eff Defects Solids 116(1–2):29–36
81. Rajta I, Szilasi SZ, Budai J, Toth Z, Petrik P, Baradacs E (2007) Nucl Instrum Methods B 260(1):400–404
82. Kudoh H, Sasuga T, Seguchi T, Katsumura Y (1996) Polymer 37(21):4663–4665
83. Lee E, Rao G, Mansur L, Balogh A, Walter G (1997) Paper presented at the international symposium on materials science applications of ion beam techniques, Seeheim
84. Kavetskyy TS, Borc J, Kukhazh YY, Stepanov AL (2015) The influence of low dose ion-irradiation on the mechanical properties of PMMA probed by nanoindentation. In: Petkov P, Tsiulyanu D, Kulisch W, Popov C (eds) Nanoscience advances in CBRN agents detection, information and energy security. Springer, Netherlands, pp 65–71
85. Venkatesan T, Forrest SR, Kaplan ML, Murray CA, Schmidt PH, Wilkens BJ (1983) J Appl Phys 54(6):3150–3153
86. Hadjichristov GB, Gueorguiev VK, Ivanov TE, Marinov YG, Ivanov VG, Faulques E (2010) J Phys Conf Ser 207(1):012022
87. Kaplan ML, Forrest SR, Schmidt PH, Venkatesan T (1984) J Appl Phys 55(3):732–742
88. Esteves C, Thomaz R, Gutierres L, Papaleo R (2013) Nucl Instrum Methods B 314:71–76